

Evidence for charge and orbital order in the doped titanates $RE_{1-x}Ca_xTiO_3$ ($RE=Y, Er, Lu$)

A. C. Komarek,¹ M. Reuther,¹ T. Lorenz,¹ A. Cousson,² P. Link,³
W. Morgenroth,^{4,5} D. Trots,^{6,7} C. Baehtz,^{6,7} and M. Braden¹

¹*II. Physikalisches Institut, Universität zu Köln, Zùlpicher Str. 77, D-50937 Köln, Germany*

²*Laboratoire Léon Brillouin, CEA/CNRS, F-91191 Gif sur Yvette Cedex, France*

³*Forschungszentrum Heinz Maier-Leibnitz (FRM-II), TU München, D-85747 Garching, Germany*

⁴*Geowissenschaften, Abteilung Kristallographie, Universität Frankfurt, Altenhöferallee 1, D-60438 Frankfurt, Germany*

⁵*Hasylab/DESY Notkestr. 85, D-22607, Hamburg, Germany*

⁶*Darmstadt Univ. of Techn., Inst. f. Mat. Science, Petersenstr. 23, D-64287 Darmstadt, Germany*

⁷*Hasylab/DESY Notkestr. 85, D-22607 Hamburg, Germany*

(Dated: November 19, 2018)

Combining macroscopic and diffraction methods we have studied the electric, magnetic and structural properties of $RE_{1-x}Ca_xTiO_3$ ($RE=Y, Er, Lu$) focusing on the concentration range near the metal-insulator transition. The insulating phase, which is stabilized by a smaller rare-earth ionic radius, exhibits charge order with a predominant occupation of the d_{xy} orbital. The charge and orbital ordering explains the broad stability range of the insulating state in $RE_{1-x}Ca_xTiO_3$ with smaller rare-earth ions. The strong modulation of the Ti-O bond distances indicates sizeable modulation of the electric charge.

The perovskite titanates $RETiO_3$ (RE a rare earth) can be considered as the one-electron analogue to the parent compounds of the cuprate superconductors with a single hole in the 3d shell [1], but the orbital degree of freedom is not quenched in the titanates. The series $RETiO_3$ exhibits a transition from an antiferromagnetic Mott insulator for $RE=La$ to a ferromagnetic insulator for smaller RE (for example $YTiO_3$) which is associated with a change in the 3d orbital occupation [1, 2]. Hole doping suppresses the Mott-insulating ground-states rendering the samples paramagnetic and metallic. However, the phase diagrams of the two most studied systems, $La_{1-x}Sr_xTiO_3$ and $Y_{1-x}Ca_xTiO_3$, differ considerably [1]. Whereas a small amount of Sr (approximately 5%) is sufficient to render $LaTiO_3$ metallic, $Y_{1-x}Ca_xTiO_3$ samples stay insulating up to Ca-doping levels of about 40% (at room-temperature) [1, 3–5]. This astonishing stability of the insulating state in the $Y_{1-x}Ca_xTiO_3$ series can only approximately be attributed to reduced electronic band widths. The smaller A-site ionic radius causes larger structural distortions which reduce the electronic band width. However, this band-width reduction seems to be insufficient to explain the remarkable stability of the insulating state up to high amounts of doping in $Y_{1-x}Ca_xTiO_3$. By using various diffraction methods on single crystals of $RE_{1-x}Ca_xTiO_3$, we elucidate the anomalous extension of the insulating state which exhibits charge and orbital ordering. This electronic order stabilizes the insulating phase similar to the phase diagrams of $Pr_{1-x}Ca_xMnO_3$ [6] and $La_{2-x}Sr_xNiO_4$ [7].

Extensive studies of the metal-insulator (MI) transition in $Y_{1-x}Ca_xTiO_3$ [3–5, 8–11] revealed remarkable properties. Samples with a Ca content at the border of metallic and insulating phases exhibit a temperature-driven MI transition from an insulating phase at high temperature towards a metallic phase at low tempera-

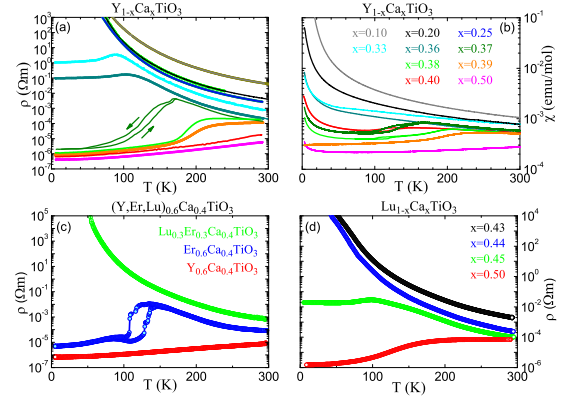


FIG. 1: (color online) The temperature dependencies of the resistivity (a) and of the magnetic susceptibility (b) in the $Y_{1-x}Ca_xTiO_3$ series, respectively. The electric resistivity is shown for various $RE_{0.6}Ca_{0.4}TiO_3$ samples in (c) and for $Lu_{1-x}Ca_xTiO_3$ in (d).

ture. This phase sequence is rather uncommon as most materials exhibit the reversed sequence with the insulating phase being stable at low temperatures. In addition, there is clear evidence for phase segregation [3, 5] with coexistence of metallic and insulating phases at low temperature. The unknown cause of the enhanced stability of the insulating state in $Y_{1-x}Ca_xTiO_3$ motivated us to perform comprehensive diffraction studies.

Untwinned single crystals of $RE_{1-x}Ca_xTiO_3$ ($RE=Y, Er, Lu$) have been grown using a floating-zone image furnace. Special effort was undertaken to control the stoichiometry which was verified by EDX analyses, by thermogravimetry and by X-ray single-crystal diffraction [12, 13]. The oxygen content determined by TGA corresponds to 3.000 ± 0.005 per formula unit for most samples studied in this work. The electrical resistiv-

ity was measured with a four-probe technique and the magnetic susceptibility by a vibrating sample magnetometer. X-ray powder diffraction data were collected on a D5000 laboratory diffractometer using Cu K_α radiation and on the beam-line B2 at the Hasylab/DESY synchrotron (wavelength 0.7495Å). Single-crystal experiments were performed with a Bruker Apex X8 diffractometer, with synchrotron radiation (beam-line D3 at the Hasylab/DESY), and with the 5C2 neutron four-circle diffractometer at the Laboratoire Léon Brillouin and with the PANDA spectrometer at FRM-II.

Figure 1 shows the temperature dependencies of the electric resistivity and of the magnetic susceptibility in $Y_{1-x}Ca_xTiO_3$. For $x=0.10, 0.20,$ and 0.25 the samples exhibit the characteristic insulating increase of electric resistivity upon cooling, but for $x=0.33$ and 0.36 the resistivity saturates towards low temperatures. Further increase of the Ca content leads to metallic behavior at low temperature with a pronounced hysteresis. The MI transition is also seen in the susceptibility which is much smaller in the metallic phase. Finally samples with $x=0.4$ and 0.5 exhibit metallic resistivity over the entire temperature range accompanied by a low magnetic susceptibility. These results agree with earlier studies[8–11]. The insulating phase is further stabilized when Y is replaced by smaller rare-earth ions, see Fig. 1(c) and 1(d). While $Y_{0.6}Ca_{0.4}TiO_3$ remains metallic till room temperature, $Er_{0.6}Ca_{0.4}TiO_3$ exhibits the MI transition at about 100K, and finally $Lu_{0.3}Er_{0.3}Ca_{0.4}TiO_3$ is insulating at all temperatures. This effect is also seen in the $Lu_{1-x}Ca_xTiO_3$ series, which exhibits the MI transition at a higher Ca content compared to $Y_{1-x}Ca_xTiO_3$, see Fig. 1(d).

Powder-diffraction data are shown in Fig. 2 for the composition $Y_{0.62}Ca_{0.38}TiO_3$. At high temperature, the diffraction patterns can be perfectly described by an orthorhombic lattice (space group Pbnm), but peaks split at low temperature indicating phase segregation. The additional phase can be described in space group Pbnm down to the lowest temperatures, but it exhibits a smaller b unit-cell parameter, see Fig. 2(b), and a smaller unit-cell volume (not shown). The original phase with the larger unit-cell volume transforms into a monoclinic phase as can be seen in the additional splitting of the corresponding peaks, see Fig. 2(a) and in the temperature dependence of the monoclinic angle β . The phase segregation and the transition into a monoclinic phase perfectly agree with a previous diffraction study on $Y_{1-x}Ca_xTiO_3$ [3, 5]. The structural transition coincides with the anomalies seen in the electric resistivity and in the magnetic susceptibility. With the temperature dependence of the volume fraction of the two phases, see Fig. 2(c), we may simultaneously describe the magnetic and resistivity data. Thereby, one can unambiguously assign the small unit-cell volume phase to the metallic phase which we label MO (metallic orthorhombic) in the following. The insulating phase thus exhibits the additional structural phase transition from the IO (insulating

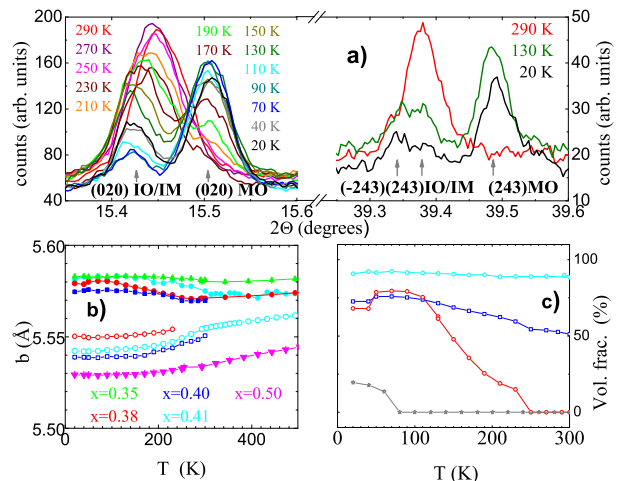


FIG. 2: (color online) (a) Diffraction patterns obtained with synchrotron radiation at beam-line B2 at HASYLAB for the sample with $x=0.38$. On the left the (020)-peaks of the insulating IO/IM phase and of the MO phase are shown for different temperatures. On the right side the (± 243) peaks are shown. As the peaks of the insulating and metallic phases are well separated, one can easily observe a splitting in the left peak indicating the transition from the IO phase to the IM phase with $\beta \approx 90.1^\circ$. (b) b lattice parameter as a function of temperature. The samples with $x=0.35$ and $x=0.38$ were measured at beam-line B2 at HASYLAB, others with a laboratory source. Open symbols denote values for the MO phase. (c) The volume ratio of the MO phase for $x=0.37$ (taken from referece [4] (black), 0.38 (red), 0.40 (blue), and 0.41 (light blue).

orthorhombic) phase at high temperature to the IM (insulating monoclinic) phase at low temperatures.

The microscopic character of the monoclinic phase has been elaborated by a series of diffraction experiments using neutron, synchrotron and laboratory X-ray radiation. Due to the b glide-mirror plane in space group Pbnm, (0kl) reflections with k odd are extinct. Neutron diffraction experiments on the PANDA spectrometer, however, show these reflections to appear at a temperature of about 150 K in $Y_{1-x}Ca_xTiO_3$ with $x=0.33, 0.35,$ and 0.36 , see Fig. 3. The (011) and (013) reflections can be transformed into cubic notation referring to the simple 3.8Å cubic perovskite cell, where they correspond to $(0.5,0.5,0.5)_{cubic}$ and $(0.5,0.5,1.5)_{cubic}$, respectively. These half-integer indexed reflections refer to a G-type distortion, i.e. a three-dimensional checkerboard ordering, which occurs in the monoclinic phase.

Full structure analyzes have been performed by single-crystal diffraction, see table I. The $Y_{1-x}Ca_xTiO_3$ crystals with $x=0.35$ and 0.36 have been studied at room temperature in the IO phase and at low temperature in the IM phase collecting large Bragg-reflection-intensity data sets on the neutron four-circle diffractometer 5C2. The refinements of the crystal structure models in space groups Pbnm and $P2_1/n$ yield no significant difference for the room-temperature data sets, but the low-

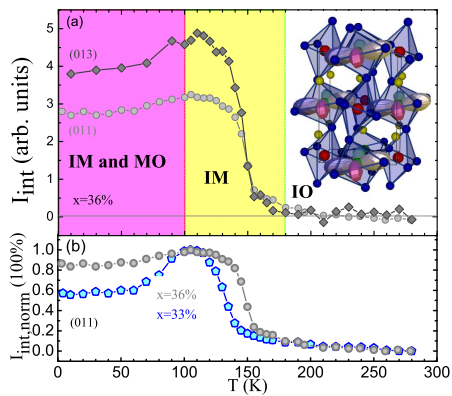


FIG. 3: (color online) (a) Intensities of the (011) and (013) superstructure reflections in Pbnm for $Y_{0.64}Ca_{0.36}TiO_3$ measured on the PANDA neutron spectrometer. The inset shows the $\sqrt{(2) \times \sqrt{(2)} \times 2}$ unit cell of the charge-ordered structure with Ti^{4+} ions (red) and Ti^{3+} ions (green) and the predominantly occupied d_{xy} orbital at the Ti^{3+} site. (b) shows the comparison of the (011) intensity measured on PANDA for $x=0.33$ and $x=0.36$.

temperature data is much better described in space group $P2_1/n$. In this lower symmetry, there are two inequivalent Ti sites, labelled Ti1 and Ti2, and two in-plane oxygen sites, labelled O2 and O2'. The structure refinements yield a clear difference in the oxygen surrounding with a larger mean Ti-O distance for the Ti2 site. Whereas the Ti1 site shows an almost isotropic bonding, the octahedron around Ti2 is flattened due to stretching of the bonds parallel to the a, b plane. These oxygen coordinations can be further analyzed by the bond-valence sum (BVS) formalism [14], where the empirical valence per bond is summed over the coordination, $Z_{BVS} = \sum_i e^{\frac{r_0 - r_i}{B}}$ with r_i the bond distance, r_0 and B empirical parameters. The BVS analysis indicates a modulation of the charge at the Ti sites by $\Delta Z=0.32(1)$ and $0.23(1)$ electron charges, for $x=0.35$ and 0.36 respectively. In addition the flattened shape of the TiO_6 octahedron around Ti2 points to an orbital ordering with a predominant occupation of the d_{xy} orbital. These structural distortions show that $Y_{1-x}Ca_xTiO_3$ in the IM phase exhibits charge ordering with additional orbital polarization occurring at the lower-valent site Ti2 (nominally $3+$). The distorted crystal structure is drawn in Fig. 3 (a).

Figure 4 presents the phase diagram of $Y_{1-x}Ca_xTiO_3$ near the MI transition. The transformation into the metallic state upon cooling is not complete but results in phase segregation and in phase coexistence. The insulating phase exhibits the additional transition into the low-temperature monoclinic phase driven by charge and orbital ordering. The charge modulation in $Y_{1-x}Ca_xTiO_3$ as obtained by the BVS calculations is smaller than one electron charge, which may not be expected as the electronic doping of these compounds is not sufficient for

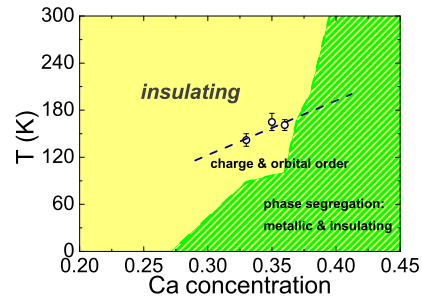


FIG. 4: (color online) Phase diagram of $Y_{1-x}Ca_xTiO_3$. MI transition temperatures were obtained from the resistivity data, and transition temperatures for charge and orbital ordering were determined in the neutron diffraction experiments. $Y_{1-x}Ca_xTiO_3$ exhibits coexistence of the metallic and the insulating phase in a broad concentration range and only highly-doped samples show an almost single metallic phase.

integer-valent checkerboard ordering. Increase of the doping stabilizes the metallic phase in $Y_{1-x}Ca_xTiO_3$ and no trace of the insulating monoclinic and charge-ordered phase can be found for $Y_{0.5}Ca_{0.5}TiO_3$ by diffraction techniques. However, the charge ordering at an electronic doping close to 50% can be studied in the compounds containing small rare-earth ions, in which the insulating phase is further stabilized, see Fig. 1(c) and 1(d). X-ray single-crystal diffraction experiments have been performed for $Lu_{0.3}Er_{0.3}Ca_{0.4}TiO_3$, $Lu_{0.56}Ca_{0.44}TiO_3$, and $Lu_{0.5}Ca_{0.5}TiO_3$ at temperatures of 8K, 125K and 10 K, respectively. For the first two data sets, the refinements significantly improve in the monoclinic space group, whereas the $Lu_{0.5}Ca_{0.5}TiO_3$ data are equally well described in space group Pbnm. This indicates that $Lu_{0.3}Er_{0.3}Ca_{0.4}TiO_3$ and $Lu_{0.56}Ca_{0.44}TiO_3$ exhibit charge and orbital ordering, but $Lu_{0.5}Ca_{0.5}TiO_3$ not, in perfect agreement with the respective behavior found in the electric resistivity, see Fig. 1(d), which shows that $Lu_{0.5}Ca_{0.5}TiO_3$ stays metallic to the lowest temperatures. Qualitatively, the structural distortions in $Lu_{0.3}Er_{0.3}Ca_{0.4}TiO_3$ and in $Lu_{0.56}Ca_{0.44}TiO_3$ agree with those in the charge ordered $Y_{1-x}Ca_xTiO_3$ compounds described above. In particular, we find the identical flattening of the octahedron around the Ti2 site which points to orbital order associated with predominant occupation of the d_{xy} orbital. The modulation of the electronic charge is, however, significantly enhanced yielding values of $\Delta Z=0.72(3)$ and $0.82(2)$ electron charges for $Lu_{0.3}Er_{0.3}Ca_{0.4}TiO_3$ and $Lu_{0.56}Ca_{0.44}TiO_3$, respectively. This enhanced electronic modulation can be attributed to the doping level close to $x=0.5$ which allows for an ideal checker-board charge order with $\Delta Z=1$.

The charge and orbital ordering in $RE_{1-x}Ca_xTiO_3$ strongly resembles the corresponding effects in several manganites. Also in $La_{1-x}Sr_{1+x}MnO_4$ [15] and in perovskite manganites [16, 17] commensurate charge and or-

bit order of the checkerboard type occurs even below the $x=0.5$ doping level. The charge and orbital ordered state becomes more stable close to the optimum doping in the manganates [15, 18] as well as in the titanates, but smaller RE ions are needed in order to overcome the trend towards metallicity in the titanates. There is also strong resemblance with the $RENiO_3$ series which exhibit a MI transition into a charge-ordered phase except for $RE=La$ [19]. The charge disproportionation in $RENiO_3$ [20, 21] is qualitatively comparable to the charge order in $RE_{1-x}Ca_xTiO_3$, but the titanates exhibit a stronger charge modulation close to the ideal half-doping. Also in the nickelate series the RE ionic radius has a strong impact on the charge ordering, as the distortions related with a smaller rare earth stabilize charge order similar to our observations for $RE_{1-x}Ca_xTiO_3$.

So far no evidence for charge ordering has been reported for any titanate bulk materials with the perovskite or with a related layered structure. However, charge order is discussed for the heterostructures involving $LaTiO_3$ and $SrTiO_3$ [22, 23]. At the interface between these two materials, the same electronic doping as for half-doped $RE_{1-x}Ca_xTiO_3$ with $x=0.5$ is realized. This interface has been studied by density-functional theory (DFT) [23] calculations which obtain a checkerboard ordering similar to our finding for the bulk material. Also the orbital ordering obtained in the DFT interface calculations

dominant occupation of the d_{xy} orbitals is found in both cases. The observation of charge and orbital order in bulk titanates near half doping gives strong support to the DFT interface calculations [23] and renders similar calculations for the bulk materials highly desirable. The electron-phonon coupling associated with the charge order in the titanates must be strong and certainly is a relevant factor also in the physics of the interfaces.

In conclusion, comprehensive diffraction studies on single crystals of $RE_{1-x}Ca_xTiO_3$ ($RE=Y, Er, Lu$) identify the origin of the monoclinic phase appearing at the insulator-to-metal crossover. Charge and orbital ordering occurs in samples with a smaller rare-earth ion and a doping level near $x=0.5$. Upon cooling, the compositions close to the doping-driven MI transition exhibit phase segregation into a metallic and an insulating phase similar to manganates exhibiting colossal magneto-resistivity. This insulating phase exhibits G-type charge order. We may thus identify charge and orbital ordering as the important element to stabilize the insulating state in the doped titanates. Charge and orbital order should be a more general phenomenon in titanate materials also relevant for the discussion of heterostructures involving $LaTiO_3$ and $SrTiO_3$.

This work was supported by the Deutsche Forschungsgemeinschaft through SFB 608. We thank H. Roth for providing three of the samples studied.

x	0.35	0.35	0.36	0.36	0.4	0.44
T(K)	120	298	110	298	8	125
radiation	n	n	n	n	synchr.	X-ray
space group	P2 ₁ /n	Pbnm	P2 ₁ /n	Pbnm	P2 ₁ /n	P2 ₁ /n
reflections	1538	1553	1790	366	17368	7853
R/R _w (%)	4.0/8.4	3.5/5.8	3.3/3.1	5.4/5.9	2.8/5.5	2.3/4.3
<i>a</i> (Å)	5.3579(1)	5.3679(1)	5.3461(1)	5.3553(1)	5.3317(5)	5.3123(2)
<i>b</i> (Å)	5.5804(1)	5.5834(1)	5.5865(1)	5.5823(1)	5.5667(5)	5.5542(2)
<i>c</i> (Å)	7.6629(1)	7.6804(1)	7.6402(1)	7.6579(1)	7.6452(5)	7.6273(3)
x(Y1/Ca1)	0.9834(1)	0.9841(1)	0.9847(1)	0.9849(2)	0.9814(1)	0.9812(1)
y(Y1/Ca1)	0.0641(1)	0.0631(1)	0.0623(1)	0.0612(4)	0.0661(1)	0.0660(1)
z(Y1/Ca1)	0.2476(2)	0.25	0.2488(3)	0.25	0.2506(1)	0.2504(1)
U(Y1/Ca1)	0.0095(2)	0.0136(2)	0.0047(1)	0.0063(7)	0.0041(1)	0.0022(1)
U(Ti1/Ti2)	0.0085(3)	0.0111(3)	0.0029(1)	0.0038(11)	0.0036(1)	0.0009(1)
x(O1)	0.1039(1)	0.1030(2)	0.0999(1)	0.1002(2)	0.1057(3)	0.1055(3)
y(O1)	0.4656(1)	0.4658(1)	0.4678(1)	0.4668(5)	0.4639(2)	0.4633(2)
z(O1)	0.2507(3)	0.25	0.2526(4)	0.25	0.2499(6)	0.2471(5)
U(O1)	0.0125(2)	0.0154(2)	0.0068(1)	0.0088(8)	0.0093(3)	0.0082(3)
x(O2)	0.6993(3)	0.6956(1)	0.7004(3)	0.6964(2)	0.7049(8)	0.699(1)
y(O2)	0.3057(2)	0.3013(1)	0.3035(3)	0.3003(3)	0.3068(7)	0.3108(5)
z(O2)	0.0554(2)	0.0529(1)	0.0493(3)	0.0517(1)	0.0553(6)	0.0491(4)
U(O2)	0.0125(2)	0.0159(1)	0.0066(1)	0.0085(6)	0.0078(3)	0.0065(3)
x(O3)	0.8079(3)	/	0.8077(3)	/	0.8155(8)	0.809(1)
y(O3)	0.7977(3)	/	0.7965(3)	/	0.7965(7)	0.7919(5)
z(O3)	0.0514(2)	/	0.0540(3)	/	0.0543(6)	0.0609(4)
U(O3)	0.0122(1)	/	0.0066(1)	/	0.0041(1)	0.0065(3)
Ti1-O1 (Å)	2.011(2)	1.993(1)	2.018(3)	1.995(1)	2.002(4)	1.976(4)
Ti1-O2 (Å)	1.991(1)	2.019(1)	1.984(2)	2.004(1)	1.952(4)	1.950(4)
Ti1-O2' (Å)	1.997(1)	2.045(1)	1.996(2)	2.005(1)	1.966(4)	1.967(3)
Ti2-O1 (Å)	2.001(2)	/	1.980(3)	/	2.003(4)	2.020(4)
Ti2-O2 (Å)	2.060(1)	/	2.044(2)	/	2.071(4)	2.059(3)
Ti2-O2' (Å)	2.041(2)	/	2.047(2)	/	2.070(4)	2.062(4)
Δ BVS	0.32(1)	/	0.23(1)	/	0.72(3)	0.82(2)

TABLE I: Crystal structure resulting from various single-crystal diffraction experiments using neutron (n), synchrotron (synchr.) or laboratory X-ray radiation on $Y_{1-x}Ca_xTiO_3$ ($x=0.35$ and 0.36), $Lu_{0.3}Er_{0.3}Ca_{0.4}TiO_3$ ($x=0.4$) and $Lu_{0.56}Ca_{0.44}TiO_3$ ($x=0.44$).

perfectly agrees with our structure analyses, as a pre-

- [1] M. Imada *et al.*, Rev. Mod. Phys. **70**, 1039 (1998).
- [2] M. Cwik *et al.*, Phys. Rev. B **68**, 060401 (2003).
- [3] K. Kato *et al.*, J. Phys. Soc. Japan **71**, 2082 (2002).
- [4] M. Tsubota *et al.*, J. Phys. Soc. Japan **72**, 3182 (2003).
- [5] H. Matsuhata *et al.*, Phys. Rev. B **70**, 134109 (2004).
- [6] Y. Tokura *et al.*, Science **288**, 462 (2000).
- [7] C. H. Chen *et al.*, Phys. Rev. Lett. **71**, 2461 (1993); J. M. Tranquada, D. J. Buttrey, V. Sachan, and J. E. Lorenzo, Phys. Rev. Lett. **73**, 1003 (1994).
- [8] F. Iga *et al.*, Physica B **206,207**, 859 (1995).
- [9] Y. Taguchi *et al.*, Phys. Rev. B **48**, 511 (1992).
- [10] F. Iga *et al.*, Physica B **223,224**, 526 (1996).
- [11] T. Tsurui *et al.*, Phys. Rev. B **69**, 024102 (2004).
- [12] H. Roth, dissertation, Univ. Cologne (2008).
- [13] A.C. Komarek, dissertation, Univ. Cologne (2009).
- [14] I. D. Brown and D. Altermatt, Acta Cryst. B **41**, 244 (1985).
- [15] S. Larochelle *et al.*, Phys. Rev. B **71**, 024435 (2005).
- [16] C. H. Chen, S.-W. Cheong, and H. Y. Hwang, J. Appl. Phys. **81**, 4326 (1997).
- [17] M. v. Zimmermann *et al.*, Phys. Rev. B **64**, 195133 (2001).
- [18] D. Senff *et al.*, Phys. Rev. B **77**, 184413 (2008).
- [19] J.B. Torrance *et al.*, Phys. Rev. B **45**, 8209 (1992).
- [20] J. A. Alonso *et al.*, Phys. Rev. Lett. **82**, 3871 (1999).
- [21] U. Staub *et al.*, Phys. Rev. Lett. **88**, 126402 (2002)
- [22] A. Ohtomo *et al.*, nature **419**, 378 (2002).
- [23] R. Pentcheva and W.E. Pickett, Phys. Rev. Lett. **99**, 016802 (2007); *ibid.*, Phys. Rev. B **74**, 035112 (2006).